

Nuclear Engineering and Technology

journal homepage: www.elsevier.com/locate/net

Original Article

A Concise Design for the Irradiation of U–10Zr Metallic Fuel at a Very Low Burnup



Haibing Guo^{*}, Wei Zhou, Yong Sun, Dazhi Qian, Jimin Ma, Jun Leng, Heyong Huo, and Shaohua Wang

Institute of Nuclear Physics and Chemistry, China Academy of Engineering Physics, No. 64 Mianshan Road, Mianyang 621999, Sichuan Province, China

ARTICLE INFO

Article history:

Received 25 April 2016

Received in revised form

24 November 2016

Accepted 7 December 2016

Available online 3 January 2017

Keywords:

CMRR

Irradiation Design

Neutron Radiography

Swelling

U–10Zr

ABSTRACT

In order to investigate the swelling behavior and fuel–cladding interaction mechanism of U–10Zr alloy metallic fuel at very low burnup, an irradiation experiment was concisely designed and conducted on the China Mianyang Research Reactor. Two types of irradiation samples were designed for studying free swelling without restraint and the fuel–cladding interaction mechanism. A new bonding material, namely, pure aluminum powder, was used to fill the gap between the fuel slug and sample shell for reducing thermal resistance and allowing the expansion of the fuel slug. In this paper, the concise irradiation rig design is introduced, and the neutronic and thermal–hydraulic analyses, which were carried out mainly using MCNP (Monte Carlo N-Particle) and FLUENT codes, are presented. Out-of-pile tests were conducted prior to irradiation to verify the manufacturing quality and hydraulic performance of the rig. Nondestructive postirradiation examinations using cold neutron radiography technology were conducted to check fuel cladding integrity and swelling behavior. The results of the preliminary examinations confirmed the safety and effectiveness of the design.

© 2017 Korean Nuclear Society, Published by Elsevier Korea LLC. This is an open access article under the CC BY-NC-ND license (<http://creativecommons.org/licenses/by-nc-nd/4.0/>).

1. Introduction

Metallic fuel has been in use for a long time in many nuclear reactors, such as the Experimental Breeder Reactor (EBR-II) and the Dounreay Fast Reactor, owing to its enhanced thermal conductivity, large fissile nuclei density, and negative temperature feedback coefficient [1]. In the United States Integral Fast Reactor program, a series of irradiation experiments were performed in the EBR-II, the Fast Flux Test

Facility, and the Chicago Pile-5 reactors to investigate the irradiation behavior of U–Pu–Zr alloy fuel [2]. The results showed that the fuel exhibited as much as 7% axial elongation when it reached a burnup of 1.5 at.% [3]. In other experiments, fuel–cladding mechanical interaction (FCMI) and fuel–cladding chemical interaction (FCCI) were studied [4]. According to previous reports, swelling of metallic fuel was mainly attributable to the accumulation of fission gas and other products, and in the event of fuel–cladding contact,

^{*} Corresponding author.

E-mail address: guohaib@caep.cn (H. Guo).

<http://dx.doi.org/10.1016/j.net.2016.12.005>

1738-5733/© 2017 Korean Nuclear Society, Published by Elsevier Korea LLC. This is an open access article under the CC BY-NC-ND license (<http://creativecommons.org/licenses/by-nc-nd/4.0/>).

the FCMI and FCCI began to affect the integrity of the cladding.

Recently, in China, a fusion–fission hybrid energy reactor (FFR) concept was proposed [5]; U–10Zr alloy was chosen as the candidate fuel. This alloy uses abundant uranium, and elemental zirconium has a weight fraction of 10%. The most important characteristic of this concept was the use of light water as the coolant and moderator. As a result of the use of light water, the neutron energy spectrum in the subcritical blanket was more moderated than that in a fusion reactor or a fast reactor, but it was harder than that in a thermal reactor. This enabled the adjustment of the production and depletion rates of fissile nuclei to maintain equilibrium, which is necessary in order to reach a much higher burnup and nuclear resource utilization rate [6]. In the FFR concept, the metallic fuel elements were recycled through a melting–casting process [7], in which approximately 38 wt.% of fission products were eliminated whereas all actinides and most long-term radioactive isotopes were preserved. The irradiation behavior of the fuel was one of the most important study topics, and hence, the U–10Zr fuel irradiation (UZFI) experiment was scheduled in the China Mianyang Research Reactor (CMRR).

This paper presents the results of neutronic and thermal–hydraulic analyses performed for the design of this experiment in a concise manner. Several nondestructive examinations and test results are explained to show the quality of the capsules and the validity of the experiment design. The postirradiation integrity of the fuel pins was checked using cold neutron radiography (CNR) technology [8]. Other postirradiation examinations (PIEs), including metallic phase observation, exact shape profiling, and measurement of thermophysical properties, are under way. The described methodology, which is used for the design of a fuel irradiation experiment in a research reactor, is general and can be applied to other cases.

2. Irradiation capsule design

2.1. China Mianyang Research Reactor

The CMRR is a pool-type research reactor owned and operated by the Institute of Nuclear Physics and Chemistry, Mianyang, China. The light water in the pool is used as the coolant; it flows downward through the core. Plate-type fuel elements are used in the reactor, and it is operated under atmospheric conditions. The coolant temperatures at the inlet and outlet of the core are 35°C and 38°C, respectively [8].

In the UZFI experiment, two center symmetric positions in the core are used for irradiation. The experiment conforms to the criteria approved by the CMRR Safety Guard Committee. The main criteria are as follows: (1) the coolant mass flow in an irradiation rig should be less than 2.78 kg/s; (2) the maximum temperature of the irradiation sample surface should be lower than 84°C; (3) the reactivity introduced by irradiation rigs should be less than 0.5% $\Delta k/k$; and (4) any factor that may lead to melting of the internal materials should be avoided.

2.2. Design of the irradiation rig

The target maximum fission burnup of uranium nuclei in the U–10Zr fuel in the UZFI experiment was 0.5 at.%, including contributions from U-235 and U-238. In order to speed up the irradiation process and allow sufficient time for the radioactivity to decay and for the conducting of PIEs, a larger fission reaction rate and consequently a faster depletion rate of fissile nuclei are required. In the research reactor, which has a thermal neutron spectrum, these requirements can be met using U-235 enriched fuel slugs.

For a specific type of fuel with a given density and heavy metal fraction, the use of enriched uranium results in higher volumetric power density (VPD). The temperature rise between the outer surface and the centerline of a cylindrical body is proportional to the linear heat rate (LHR) and is independent of the radius. So, the thermal criteria will basically provide a restriction to the value of LHR, which is obtained by integrating VPD over the cross-sectional area. If VPD is expected to be high, in order to satisfy the thermal criteria, the fuel slugs were required to have small cross-sectional areas. Considering the convenience of mechanical fabrication and remote handling during PIEs, the dimensions of a fuel slug were set at $\phi 5 \times 15$ mm, which is almost the lower limit of mechanical fabrication and remote handling.

Two types of irradiation samples and capsules were designed to investigate the free swelling behavior and fuel–cladding interaction, respectively. Schematic pictures of samples and their computer tomography and digital radiography (CT–DR) images are shown in Fig. 1. The main parameters are listed in Table 1, in which the smeared density is estimated by the ratio of the cross-sectional area of fuel slug to the total inner cross-sectional area of the cladding. The space occupied by the solid grain of aluminum powder is eliminated from the total inner cross-sectional area.

Molten salts (such as FLiBe and FLiNaK) or molten metals (such as sodium, lead, lead–bismuth eutectic, and lead–lithium) were not selected as the bonding material considering the low-temperature environment in the water-cooled core and the corrosion of other materials. Instead, pure aluminum powder was chosen to fill the gap between the inner slug and the sample shell. This material had two functions: (1) it acted as a thermal bond that enhanced thermal conduction, and (2) it worked as a buffer against fuel swelling.

The aluminum powder was loosely filled to 68% of the theoretical density with almost homogeneous porosity in the 1.5-mm-thick gap. The porosity decreases when an external force acts on the powder, because aluminum is soft and can even be extruded when the temperature approaches 168°C. This is because, when heating a metal, well before its melting point the recrystallization process will increase the ductility and decrease the resistance. The recrystallization temperature of aluminum is approximately $0.46 T_m$, where T_m is the melting temperature of aluminum in units of K. Furthermore, aluminum powder poses little risk to the water-cooled reactor and has a lower radioactive dose after irradiation when cooled for a short time. Consequently, with properly designed

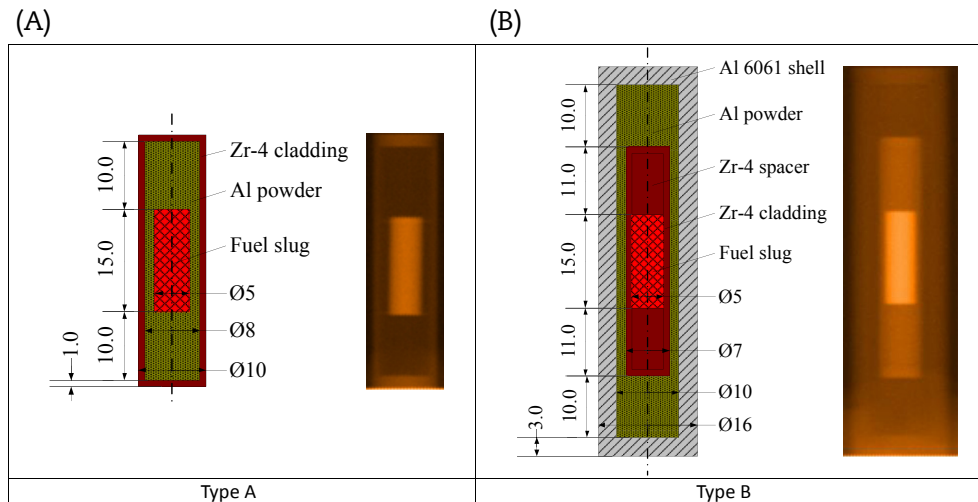


Fig. 1 – Schematic view of the samples and their CT-DR photographs. CT-DR, computer tomography and digital radiography.

volume and thickness, the porous aluminum powder can effectively accommodate the fission gas and tolerate the swelling of the fuel slug.

Following a previous study [9], we estimated that the U–10Zr fuel may exhibit approximately 2% maximum axial elongation under the irradiation condition of the UZFI experiment. However, it was difficult to estimate the radial expansion by considering only the burnup [10]. The low irradiation temperature condition in the UZFI experiment would not cause as much radial swelling as reported in the literature [11]. The smeared density data of the Type A sample in Table 1 shows that the void space in aluminum powder is approximately 0.5 times of the area of fuel slug in the radial cross section. This means that a maximum of 50% volume swelling of the fuel slug is allowed, namely, 22.5% linear expansion in the radial direction. That is enough for the safety and free swelling requirements.

All the claddings and shells are enclosed by welding. CT-DR and helium mass spectra technology were used to detect any possible defects or leakage. In the type B samples, two Zr-4 spacers were placed at each end of the fuel slug to extend the length of the cell for remote handling flexibility while

cutting. The fuel slug and spacers were tightly bonded with the cladding by thermoexpansion and shrink.

A total of 12 samples were irradiated in two rigs; every sample was placed in an individual capsule (the capsules were made of Al 6061 alloy). The samples were classified into four groups, with one group per burnup step. Every two groups, including four type A and two type B samples, were inserted in one irradiation rig. The capsules for the two types of samples had similar structures, as shown in Fig. 2—the outer diameter, flow channel width, and sizes of the positioning ribs were identical, but the height and inner cavity diameter of the capsules for the two types were different.

The sidewall of a capsule had three holes for placing Al–0.1 wt.% Co activation wires, which were used to measure the burnup of fuel slugs. The four sharp bulges at the top of the capsule match notches at the bottom of the capsule placed above. These bulges and notches ensure that the positioning ribs of all capsules are aligned, consequently minimizing the flow resistance of the coolant. The slope on each end enabled automatic matching of two adjacent capsules when randomly inserting a capsule into the rig.

Table 1 – Sample parameters.

Parameters	Type A	Type B
Fuel slug dimensions (mm)	$\phi 5 \times 15$	$\phi 5 \times 15$
Fuel composition	U–10 wt.% Zr	U–10 wt.% Zr
Nominal fuel density (g/cm ³)	16.03	16.03
Uranium loading per fuel slug (g)	4.25	4.25
Zircaloy-4 (Zr-4) cladding thickness (mm)	1.0	1.0
Aluminum (Al) shell thickness (mm)	—	3.0
Al powder thickness in the radial direction (mm)	1.5	1.5
Al powder depth at the two ends (mm)	10	10
Porosity of the Al powder (%)	32	32
Sample dimensions (mm)	$\phi 10 \times 37$	$\phi 16 \times 63$
Smeared density (planar) (%)	66.7	100 (100)
Target of irradiation	Free swelling behavior	Fuel–cladding interaction
Destination burnup in atomic fraction (%)	0.1, 0.3, 0.5, 0.7	0.1, 0.3, 0.5, 0.7
Number of samples	8, 2 for each burnup step	4, 1 for each burnup step

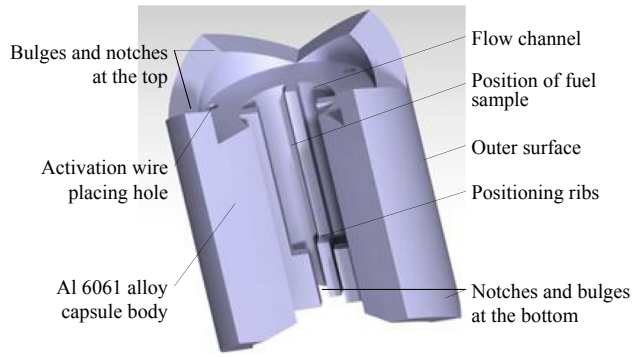


Fig. 2 – Schematic view of the irradiation capsule design.

The arrangement of capsules in an irradiation rig is shown in Fig. 3. An aluminum spacer, placed on the top of all capsules, had two effects: it formed a flow channel to control the flow rate, and it acted as a space occupier to control the amount of the neutron moderator, i.e., water. The capsules were loaded and discharged in the hot cell by remote handling. Thereafter, the two irradiation rigs were transferred into the CMRR core for irradiation, or transferred to other hot cells for PIEs.

3. Neutronic and thermal–hydraulic analysis

Two parameters were yet to be determined in the design phase: the enrichment level of U-235 in the fuel slug and the cooling channel width. Higher enrichment was preferred to obtain higher VPD and shorter irradiation time. However, a series of thermal limits restricted the LHR of fuel slugs, implying that the enrichment has an upper limit. The cooling channel width was restrained both by the cooling capability requirement and the mass flow rate criterion.

The two types of samples had to conform to the same surface temperature criterion, which can be expressed by the difference between the surface temperature and the bulk coolant temperature. An estimation of that temperature difference is shown in Eq. (1).

$$\Delta T = \frac{q'}{\pi d_s h} = \frac{q'}{\pi \lambda \text{Re}^a \text{Pr}^b} \propto \frac{q'}{W^a} \delta^a \left(\frac{\delta}{d_s} + 1 \right)^a, \quad (1)$$

where q' is the LHR; d_s is the outer diameter of the sample; h is the heat transfer coefficient; λ is the thermal conductivity of the coolant; W is the coolant flow rate; and δ is the cooling

channel width; furthermore, C , a , and b are constants for the heat transfer coefficient estimation.

For samples in one irradiation rig, the coolant flow rates W were identical, and the LHR q' values differed slightly. For samples of both type A and type B, the quantity δ/d_s was relatively small, and the values were very close. Hence, the difference in ΔT between the different types of samples was determined by considering the cooling channel width δ .

In order to meet the temperature criterion, the cooling channel widths of the two types of samples were set to be identical. Hence, the flow area of the type A capsules was smaller than that of the type B capsules, and the corresponding mass flow flux and heat transfer coefficient were larger in the type A capsules. However, the heat transfer area of the type A samples was smaller, and the corresponding heat flux was larger. The combination of these two effects resulted in identical ΔT values for both types of samples.

In the following subsections, the cooling capability and flow rates of the irradiation rig with different cooling channel widths, and a determination of the optimum values, are described. Furthermore, the LHR limits of fuel slugs are derived, and a series of neutronic calculations to determine the enrichment of U-235 in fuel slugs are explained.

3.1. Coolant flow rate design and verification

The coolant flow rate of an irradiation rig has an upper limit, as approved by the CMRR Safety Guide Committee ($<2.78 \text{ kg/s}$). In addition, the flow rate is restricted by the cooling capability requirement and flow resistance performance. A series of detailed three-dimensional (3D) models of the irradiation rig with different cooling channel widths were established, and these were imported into the computational fluid dynamics (CFD) code FLUENT to conduct mass flow rate simulations [12]. The simulations were carried out under a common boundary condition of 110 kPa pressure drop from rig top to bottom, because the pressure drop in the CMRR core is about 110 kPa, and this does not change after the insertion of the rig.

In the annular flow channel, both the Dittus–Boelter and Sieder–Tate correlations are insufficient to evaluate the heat transfer coefficient. Instead, a correlation derived by Dirker and Meyer [13] is used here, as shown in Eq. (2). Certainly, Eq. (2) cannot predict the heat transfer coefficient exactly yet. We used it only to find the dependence of the heat transfer coefficient on the flow channel width, and further to determine the LHR limit. The final thermal analysis was carried out using the 3D CFD method.

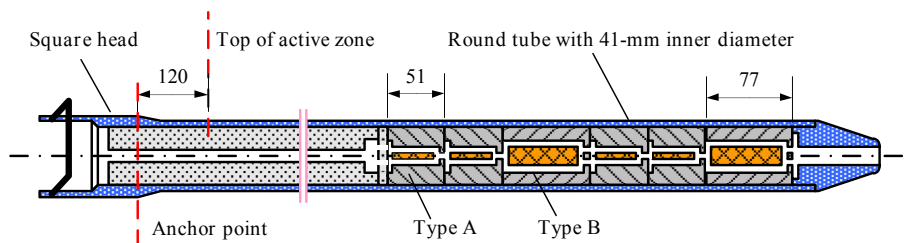


Fig. 3 – Schematic of the irradiation rig.

$$\text{Nu} = \frac{hD_e}{\lambda} = \text{CRe}_{D_e}^P \text{Pr}^{1/3} \left(\frac{\mu}{\mu_w} \right)^{0.14} = C \left(\frac{GD_e}{\mu} \right)^P \left(\frac{\mu c_p}{\lambda} \right)^{1/3} \left(\frac{\mu}{\mu_w} \right)^{0.14}, \quad (2)$$

where h is the heat transfer coefficient; D_e is the equivalent hydraulic diameter of annulus, equal to the difference between the outer and inner diameter of the annulus; and G is the coolant mass flow flux; furthermore, μ , μ_w , c_p , and λ are the thermophysical parameters of water; C and P are coefficients, as follows:

$$P = 1.013 \exp(-0.067R) \quad (3)$$

$$C = \frac{0.003R^{1.86}}{0.063R^3 - 0.674R^2 + 2.225R - 1.157}, \quad (4)$$

where R is the annular diameter ratio, i.e., the outer diameter of the annulus divided by the inner diameter of the annulus.

The thermophysical properties of the coolant, except μ_w , were obtained under the condition of 0.112 MPa and 35°C because the increase in the coolant temperature in the irradiation rig was negligible. μ_w was obtained under the condition of 0.112 MPa and the local temperature of the sample surface. The results of the mass flow rate and heat transfer coefficient for the two types of samples are shown in Fig. 4.

Fig. 4 shows that the mass flow rate increases with the cooling channel width δ . When $\delta = 6$ mm, the mass flow rate is still within the approved limit. However, the heat transfer coefficient has a maximum value at approximately $\delta = 3.4$ mm for the type A samples and at $\delta = 4.0$ mm for the type B samples. This existence of this maximum value is attributed to the increase in the flow area, which is faster than the increase in the mass flow rate as the cooling channel widens; hence, the flow flux and consequently the heat transfer coefficient decrease when the width δ is sufficiently large.

From the perspective of neutronics, less water will make the neutron spectrum less moderated, and a higher U-235 enrichment can be realized at the same power limit. In such a case, when fuel slugs reach deep burnup, the fraction of depleted U-235 is small, and the VPD and burnup rate do not

decrease significantly. Hence, the cooling channel width was set at 3.0 mm, and the mass flow rate, estimated using the CFD method, was approximately 0.854 kg/s.

Prior to in-core irradiation, a group of mockup samples and capsules were manufactured to conduct an out-of-pile flow resistance experiment. The mockup samples were made of solid aluminum, with the same size as the irradiation samples. Six mockup samples and capsules were inserted into the irradiation rig in the planned order, and the pressure drops between the rig top and tail were measured at different water flow rates. The results are shown in Fig. 5.

For the in-core pressure drop condition, the mass flow rate of coolant in the irradiation rig was 0.953 kg/s. The estimated value, calculated by the CFD method, is approximately 10% less than the actual value. The overestimation of the flow resistance by the CFD method is attributed to the numerous right angles and protruding bodies in the model; the angles were rounded in the actual samples and capsules. It was difficult to describe the small rounding in the CFD model and the meshes.

Based on the actual mass flow rate of the coolant, the heat transfer coefficients were estimated using Eqs. (2–4) for the type A and B samples; the values were 42,617 W/m² K and 29,203 W/m² K, respectively. The onset of nuclei boiling (ONB) temperature was estimated based on the Jens-Lottes correlation and the actual mass flow rate. The ONB temperature was about 20°C higher than the temperature criterion of the sample surface.

3.2. LHR limit

We needed to check that the temperatures at the interfaces of materials and at the centerline of fuel slugs conformed to the required criteria. The theoretical expressions for temperatures at these specific radial locations were derived in 1D cylindrical coordinates. In the type B samples, more structure elements were involved, and the thermal resistance from the centerline to the cooling surface was larger than that in the type A samples. Hence, we explain the relations for the type B samples in this paper; the expressions are given in Eqs. (5–9).

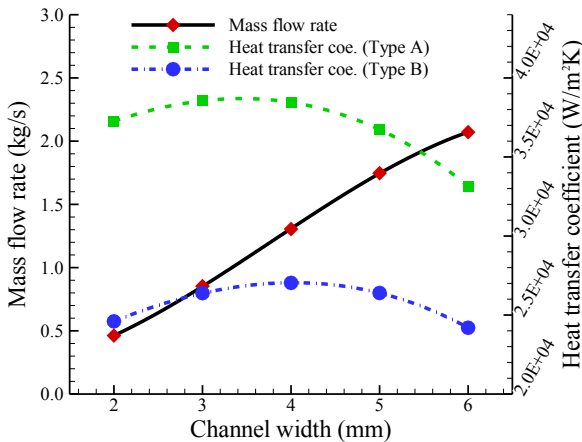


Fig. 4 – Mass flow rate and heat transfer coefficient at different channel widths. coe., coefficient. LHR, linear heat rate.

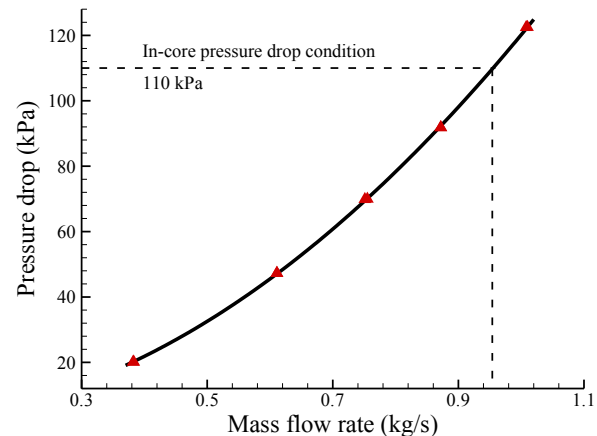


Fig. 5 – Flow resistance performance of the rig.

$$T_{\text{wall}} = T_{\text{cool}} + \frac{q'_f + q'_c + q'_b + q'_s}{2\pi R_s h} \quad (5)$$

$$T_{\text{shell}} = T_{\text{wall}} + \frac{1}{2\pi\lambda_s} \left[q'_s \left(\frac{1}{2} - \frac{R_b^2}{R_s^2 - R_b^2} \ln \frac{R_s}{R_b} \right) + (q'_f + q'_c + q'_b) \ln \frac{R_s}{R_b} \right] \quad (6)$$

$$T_{\text{bond}} = T_{\text{shell}} + \frac{1}{2\pi\lambda_b} \left[q'_b \left(\frac{1}{2} - \frac{R_c^2}{R_b^2 - R_c^2} \ln \frac{R_b}{R_c} \right) + (q'_f + q'_c) \ln \frac{R_b}{R_c} \right] \quad (7)$$

$$T_{\text{clad}} = T_{\text{bond}} + \frac{1}{2\pi\lambda_c} \left[q'_c \left(\frac{1}{2} - \frac{R_f^2}{R_c^2 - R_f^2} \ln \frac{R_c}{R_f} \right) + q'_f \ln \frac{R_c}{R_f} \right] \quad (8)$$

$$T_{\text{fuel}} = T_{\text{clad}} + \frac{q'_f}{4\pi\lambda_f}, \quad (9)$$

where T_{cool} and T_{wall} represent the temperatures of the coolant and the sample outer surface, respectively. T_{shell} , T_{bond} , and T_{clad} represent the inner surface temperature of the sample shell, the aluminum powder bonding layer, and the cladding, respectively. T_{fuel} represents the temperature at the fuel slug centerline. The subscripts s, b, c, and f indicate the sample shell, bonding layer, cladding, and fuel, respectively.

Constant thermal conductivities were assumed for all structural materials because the changes were negligible under the experiment conditions. The conductivity of the aluminum shell was set at 167 W/m K, and that of the Zr-4 cladding was set at 21.5 W/m K [14]. The thermal conductivity of aluminum powder is given in Eq. (10) [15], and that of U-10Zr fuel is given in Eq. (11) [16].

$$\lambda_b = \lambda_{\text{Al}} \left[1 - \frac{3(1-\varepsilon)(\lambda_{\text{Al}} - \lambda_{\text{air}})}{3\lambda_{\text{Al}} - \varepsilon(\lambda_{\text{Al}} - \lambda_{\text{air}})} \right] \quad (10)$$

$$\lambda_f = 3.26631 \times 10^{-6} T^2 + 2.24774 \times 10^{-2} T + 9.62036, \quad (11)$$

where λ is in units of W/m K, and T is in K. Furthermore, ε is the volume fraction of aluminum powder in the bonding gap of the sample, and it was controlled at 68%. λ_{air} represents the

thermal conductivity of air in the powder and is set at 0.02 W/m K. λ_{Al} represents the thermal conductivity of the aluminum grain. Generally, the grain is covered by a thin layer of alumina of thickness of approximately several nanometers; the thermal conductivity of this layer is approximately 30 W/m K. Considering the grain size to be 100-nm grade, the effective thermal conductivity of the aluminum grain was estimated to be 122.3 W/m K. Furthermore, the thermal conductivity of the aluminum powder was estimated to be 71.7 W/m K.

The heating rates of the structural materials in the irradiation rig were calculated using the MCNP (Monte Carlo N-Particle) 5 code. The VPD of aluminum is approximately $3 \pm 1.0\%$ W/cm³, and that of Zr-4 is approximately $12 \pm 1.6\%$ W/cm³. The data following the mean values are the relative standard deviation. These values did not vary substantially between different enrichment levels of U-10Zr samples or axial positions because the heating of the structural materials is mainly attributed to gamma irradiation, which is dominantly generated by the reactor core and is hardly affected by the materials in the irradiation rig. The aluminum powder bond has a solid fraction of 68% and, hence, an average VPD of $2 \pm 1.3\%$ W/cm³ was attained.

Based on these conditions and through iterative calculations, the temperatures of the points of interest can be obtained with respect to the LHR. The results and the adequate LHR limit of the samples are shown in Fig. 6.

Fig. 6 shows that the most crucial limits for the two types of samples are the temperatures of the outer surface and of the fuel centerline, respectively. The temperature of the type A sample wall exceeds the approved criterion of 84°C when the LHR of a fuel slug exceeds 617 W/cm, corresponding to a VPD of 3,142 W/cm³. Considering the uncertainty in the thermal conductivity of fuel and aluminum powder, and the accuracy of Eqs. (2–4), a safety margin should be reasonably set for the actual LHR limit.

3.3. Neutronic analysis

For the above-described structure design, the only quantity to be determined now is the level of U-235 enrichment of the fuel slugs. The MCNP code with ENDF/B-VI.6 cross-section

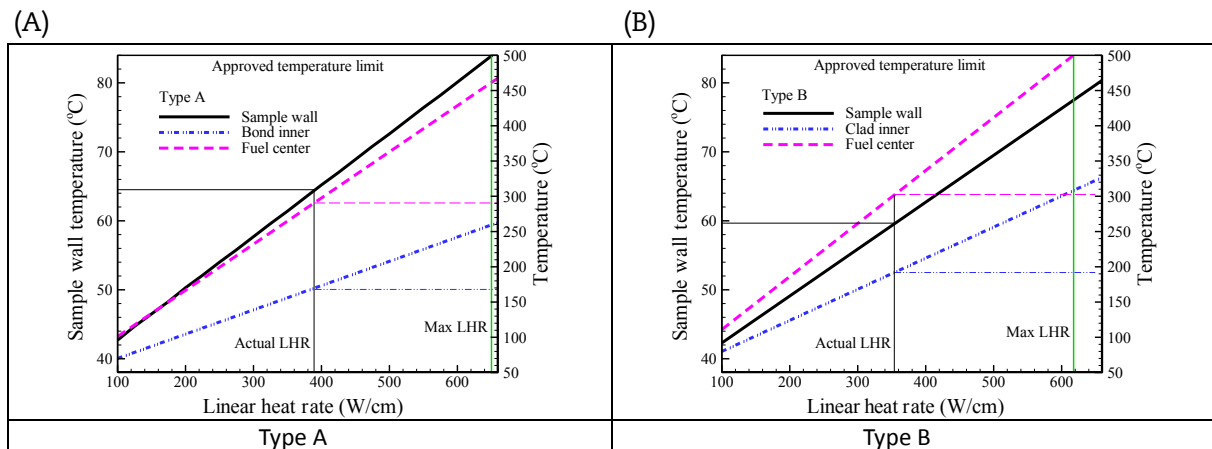


Fig. 6 – Temperatures at specific positions when fuel LHR varies. LHR, linear heat rate.

library was used to calculate the neutronic performance of the fuel slugs with different levels of U-235 enrichment [17]. High-fidelity neutronic models were established, and the simulations were carried out in the whole core domain with all the fuel elements, control rods, irradiation rigs, coolant, and reflectors included. The point burnup code ORIGEN-S was coupled with the MCNP code to account for the depletion of fuel and the reshaping of the neutron flux.

The maximum VPD and the time needed to attain a fission burnup of 0.5 at.% are listed in Table 2. An enrichment of 6 wt.% was adopted to make sure that the thermal safety margin was sufficient and that the temperatures of the fuel slugs were suitable. Furthermore, the neutronic self-shielding effect was not significant and the required irradiation time was not very long at this enrichment.

For the final design, more parameters, including the VPDs and actual fission burnup after the scheduled period of irradiation, were obtained. Some neutronic parameters are listed in Table 3; the samples are identified by the irradiation position in the core, sample type, and the arrangement order from top to bottom of the rig. The total reactivity introduced by the two U-10Zr irradiation rigs was approximately $0.07 \pm 0.02\%$ $\Delta k/k$, which was rather small and met the reactivity insertion criterion.

After a group of samples has undergone a complete irradiation course, they will be discharged, and the position will be occupied by a newly inserted aluminum spacer. The total power of an irradiation rig is less than 3.8 kW, including 0.4 kW contributed from the structure materials and aluminum spacers. The increase in coolant temperature was estimated to be approximately 0.9°C.

The radioactivity and decay heat of the discharged samples were calculated using the ORIGEN-S code with the ENDF/B-VI.6 data library. The results are shown in Fig. 7. After a cooling period of 60 days, the radioactivity of the sample was found to decrease to less than 9.25×10^{11} Bq, and the decay heat was approximately 0.1 W.

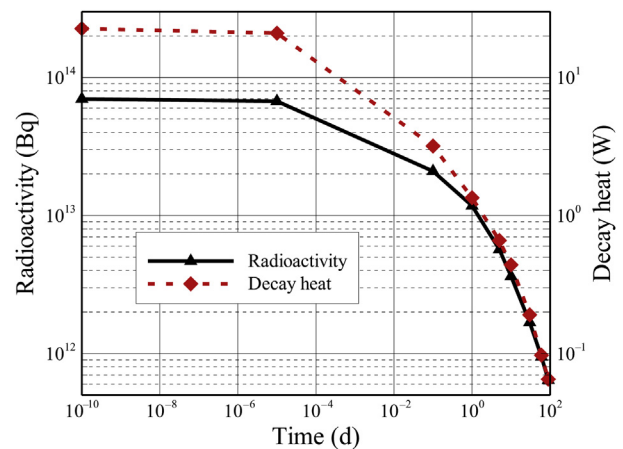


Fig. 7 – Decay heat and radioactivity of a fuel sample at 0.7 at.% burnup.

3.4. Thermal–hydraulic analysis

The maximum temperature of the U–10Zr fuel slugs was controlled at under 500°C, which provides sufficient thermal safety margin relative to the first phase transition temperature of 617°C.

3.4.1. Thermophysical properties of the materials

The thermal conductivities of the aluminum powder and the fuel are given in Eqs. (10) and (11), following data from previous studies. In calculating the aluminum powder conductivity, the thin layer of alumina coating on the grain was considered and, thus, the effective conductivity decreased. The nominal conductivities for the bonding powder and fuel at a temperature of 300°C are approximately 71.7 W/m K and 25.6 W/m K, respectively. The thermal conductivities of the Zr-4 cladding and of the aluminum shell are assumed to be constant at 21.5 W/m K and 167 W/m K, respectively.

Table 2 – Power density and time needed to reach the designated burnup.

U-235 enrichment (%)	2	4	6	8	10
Maximum VPD (W/cm ³)	820.0 ± 3.8%	1,563.6 ± 4.0%	1,981.8 ± 3.3%	2,521.7 ± 4.0%	2,790.3 ± 4.0%
Required time (d)	71.4	37.5	29.6	23.2	21.0

VPD, volumetric power density.

Table 3 – Neutronic parameters of the UZFI experiment.

Sample ID	VPD (W/cm ³)	Time (d)	Burnup (at.%)	Sample ID	VPD (W/cm ³)	Time (d)	Burnup (at.%)
P1-A1	1,596.7 ± 3.2%	4.7	0.06	P2-A1	1,416.9 ± 3.3%	14.8	0.18
P1-A2	1,717.7 ± 3.1%		0.07	P2-A2	1,729.0 ± 3.1%		0.22
P1-B1	1,802.1 ± 2.9%		0.07	P2-B1	1,759.7 ± 3.0%		0.22
P1-A3	1,981.8 ± 2.9%	23.6	0.40	P2-A3	1,901.8 ± 2.9%	33.2	0.54
P1-A4	1,925.2 ± 2.9%		0.39	P2-A4	1,925.6 ± 2.9%		0.55
P1-B2	1,770.9 ± 3.0%		0.36	P2-B2	1,731.0 ± 3.1%		0.49

UZFI, U–10Zr fuel irradiation; VPD, volumetric power density.

According to a previous study [18], the thermal conductivity of fuel changes significantly with burnup. However, the conductivity decreases less than 3.5% when the local burnup is lower than 0.56 at.% [19]. In the UZFI experiment, the maximum contribution from the fuel slug to the temperature difference between the coolant and the centerline was 47.3%. Consequently, the maximum uncertainty of the fuel temperature due to burnup is approximately 1.7%, or 5°C.

The global temperature rise of the coolant from the inlet to the outlet was approximately 0.9°C, which is negligible. As the thermophysical properties of water are not sensitive to the experiment pressure range, they were treated as constants. The density, thermal conductivity, specific capacity, and dynamic viscosity values were obtained from the International Association for the Properties of Water and Steam Industrial Formulation 1997 (IAPWS-IF97) framework table [20] under the conditions of 0.112 MPa and 35°C.

3.4.2. Simulation and results

Finally, a 3D steady-state CFD simulation was carried out using the FLUENT code. Because the irradiation rig and capsules were symmetric, a 1/8 geometry was modeled. All the capsules and aluminum spacers were modeled with high fidelity, and the coolant flow channel was modeled using Boolean subtraction and was finely meshed with tetragonal and hexagonal elements.

A segregated solver and implicit formulation were used, and the energy option was activated. The standard $k-\epsilon$ two-equation model, standard wall functions, and default constants were used to account for turbulence. Constant flow rate condition was applied for the inlet, and outflow boundary condition was applied for the outlet. The heat loadings of all bodies were set separately according to the neutronic results; the walls were assumed to be no-slip walls. The first-order upwind scheme was applied to solve the momentum equations, and the discretization of the energy equation followed the second-order scheme. Pressure–velocity coupling was accomplished using the semi-implicit method for pressure-linked equations (SIMPLE) method.

Temperature distribution results are shown in Fig. 8; the velocity magnitudes are shown in Fig. 9.

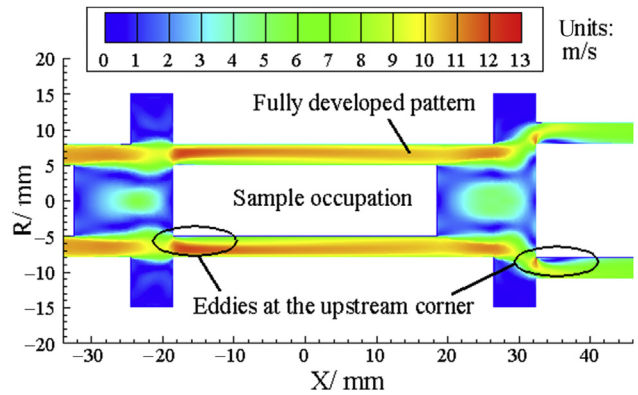


Fig. 9 – Coolant velocity magnitude distribution in a typical segment of the cross section.

The maximum temperatures of the fuels in type A and B samples were 264°C and 282°C, respectively, which corresponded to samples P1-A3 and P1-B1, respectively. The maximum temperature of the cladding in the type B samples was approximately 177°C; the maximum temperature of the aluminum powder bond in type A samples was approximately 150°C. The maximum heat flux on the sample outer surface of type A was approximately 1.11 MW/m², whereas that of type B was only 0.54 MW/m². The shell surface temperature of type A samples was approximately 56.4°C, whereas it was 50.2°C in type B samples. All of the quantities met the thermal criteria and had sufficient safety margin.

All values predicted by the CFD method were smaller than those predicted by the radial 1D analytical methods. The 1D method and its results are described in Section 3.2, which shows that the temperatures of the fuel centerline and the sample surface are 20°C and 8°C, respectively, higher than the results obtained using the CFD method. This was attributed to the axial heat conduction in the samples and to the difference in the heat transfer coefficients. Because the aluminum and bonding powder in the samples have relatively large thermal conductivity, the axial heat conductions in these areas are significant. The heat transfer coefficient estimated using Eqs. (2–4) could not take into account the entrance effect, whereas

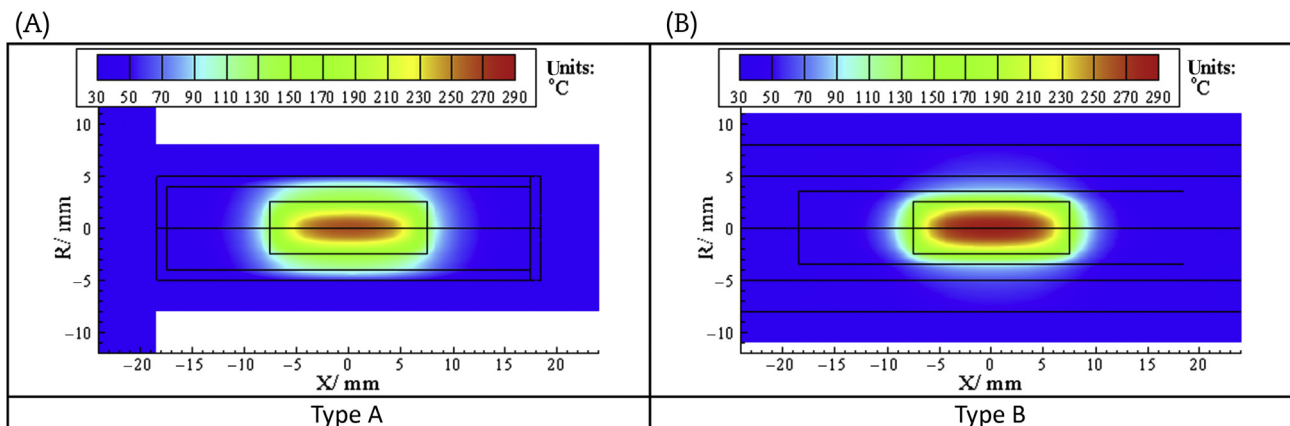


Fig. 8 – Cross-sectional temperature distribution of two types of sample.

the flow pattern around the samples was not fully developed, as shown in Fig. 9. A high-fidelity CFD simulation was able to predict the thinner heat boundary layer and eddies near the entrance of the flow channel around the sample. The sharp angles at the upstream corner of the sample enhanced the entrance effect, which resulted in the significant difference between the two calculation methods. The sharp angles in the CFD model are absent in the actual samples.

3.5. Thermal analysis of abnormal cases

Two abnormal cases were considered in the safety analysis: (1) a temporal increase in reactor power and (2) a decrease in the coolant flow rate. Because the actual VPD is much lower than the crucial value, the safety margin for the reactor power is more than 50%, which is much higher than the reactor protection limit. Hence, temporal increase in the reactor power poses little risk to the UZFI experiment.

If the coolant flow rate decreases, the heat transfer coefficients decrease as a consequence. As a result, the temperatures of the samples increase rapidly. Because the temperature difference between the centerline and the sample surface is not large, the point that first exceeds the thermal criteria will be the sample surface. According to the maximum



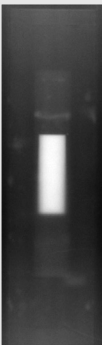





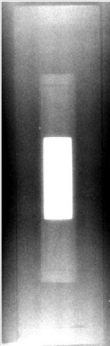


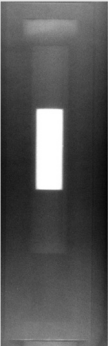
heat flux on the outer surface of the samples, the minimum heat transfer coefficients required for type A and type B samples are approximately 22,653 W/m² K and 11,020 W/m² K, respectively. And the corresponding lower limit of the mass flow rate is 0.475 kg/s. This means that the irradiation rig can tolerate a coolant flow rate decrease of 50%.

4. Preliminary PIE results

During the preliminary PIEs, the CNR facility at the CMRR was used to investigate swelling and possible cracks in the discharged samples. The CNR is an advanced nondestructive examination technology that uses large differences in the cold neutron attenuation coefficients of different materials. The samples can be investigated through remote handling at any time without worrying about radioactivity. CNR images and swelling data for the discharged samples are presented in Table 4.

The error in the size of the original samples is approximately ± 0.001 mm, and the absolute spatial resolution of the CNR images is approximately 0.05 mm. Hence, the error in the measurement of the size difference between the pre- and postirradiation samples is ± 0.051 mm. Therefore, the

Table 4 – CNR images and swelling data of all samples.

Irradiation time (d)	4.7			14.8		
Sample ID	P1-A1	P1-A2	P1-B1	P2-A1	P2-A2	P2-B1
CNR images						
Maximum swelling in the radial direction (%)	0.1	0.4	−0.5	0.8	2.3	−0.2
Maximum swelling in the axial direction (%)	1.06	0.99	0.37	1.19	2.41	−0.03
Irradiation time (d)	23.6			33.2		
Sample ID	P1-A3	P1-A4	P1-B2	P2-A3	P2-A4	P2-B2
CNR images						
Maximum swelling in the radial direction (%)	3.2	8.9	0.3	10.6	9.5	1.4
Maximum swelling in the axial direction (%)	2.39	2.72	1.75	2.00	2.30	0.99

CNR, cold neutron radiography.

relative errors in the swelling in the radial and axial directions were $\pm 1.0\%$ and $\pm 0.34\%$, respectively.

Three fuel slugs—P1-A4, P2-A3, and P2-A4—exhibited notable swelling, and one slug, P1-A3, exhibited slight swelling. All four of these samples lacked a cladding and attained a relatively high burnup. Hence, the swelling developed to a high level and was exhibited without restraint. By contrast, the two type B samples at the same burnup did not exhibit any noticeable swelling because the claddings strongly restrained the swelling of the fuel slugs, indicating mechanical interaction between the fuel and the cladding. This interaction was investigated in a later, destructive examination procedure.

The preliminary results show that the integrity of all irradiation samples was confirmed, and that the objective phenomena were observed. Further examinations of all the fuel slugs and claddings are under way to obtain an exact description of the swelling and fuel–cladding interaction.

5. Conclusion

An integrated and strictly derived method for the concise design of U–10Zr metallic fuel sample irradiation in a research reactor is introduced in this paper. This method was successfully implemented in the CMRR. In particular, to reduce the thermal resistance and allow the swelling of the fuel slug, aluminum powder was used instead of molten salts or molten metals as the bonding material between the fuel slug and the sample shell. Nondestructive examinations by CT-DR prior to irradiation and CNR technology after irradiation were used to check the quality and integrity of the fuel cladding. The primary PIE results showed that the experiment was completed safely with no structural failure or cladding rupture, and that the objective phenomena were exhibited; thus, the validity of the experiment design was confirmed. Further PIEs for research of material behavior in the field of mechanics are under way.

Conflicts of interest

We declare that we have no conflict of interest.

Acknowledgments

This work was supported by the National Magnetic Confinement Fusion Science Program of China (2015GB108001) and the National Natural Science Foundation of China (Grant No. 11405153). We greatly appreciate Dr Yuting Zhang and Dr Jianping Jia from the Science and Technology on Surface Physics and Chemistry Laboratory for preparing the U–10Zr samples. We thank Professor Bin Liu for manufacturing the irradiation capsules and rigs.

REFERENCES

- [1] H. Tsai, A.B. Cohen, M.C. Billone, L.A. Niemark, Irradiation performance of U–Pu–Zr metal fuels for liquid-metal-cooled reactors (Report No. ANL/ET/CP-82776), Argonne National Laboratory, Illinois, USA, 1994.
- [2] D.R. Pedersen, L.C. Walters, Metal fuel manufacturing and irradiation performance, Presented at the American Power Conference, 1992. Illinois, USA.
- [3] E.R. Cramer, A.L. Pitner, In situ observation of axial irradiation growth in liquid-metal reactor metal fuel, Presented at the 1989 Winter Meeting of the American Nuclear Society, 1989. San Francisco, USA.
- [4] C. Nam, W. Hwang, D. Sohn, Statistical failure analysis of metallic U–10Zr/HT9 fast reactor fuel pin by considering the Weibull distribution and cumulative damage fraction, *Ann. Nucl. Energy* 25 (1998) 1441–1453.
- [5] M. Li, R. Liu, X. Shi, X. Peng, Preliminary design of hybrid energy reactor and integral neutron experiments, *Fusion Eng. Des.* 87 (2012) 1420–1424.
- [6] H. Guo, X. Peng, X. Shi, J. Ma, Thermal–hydraulic conceptual design of water-cooled blanket of a fusion-fission hybrid reactor for energy production, *Proceedings of the 21st International Conference On Nuclear Engineering (ICONE21)*, Chengdu, 2013. ID: 15416.
- [7] H. Ohta, T. Ogata, T. Yokoo, M. Ohgier, J.P. Glatz, B. Fontaine, L. Breton, Low-burnup irradiation behavior of fast reactor metal fuels containing minor actinides, *Nucl. Technol.* 165 (2009) 96–110.
- [8] C. Hu, W. Shen, J. Dai, X. Liu, V. Kouzminov, V. Mityukhlyayev, A. Serebrov, A. Zakharov, Cold neutron source at CMRR, *Proceedings of the 9th Meeting of the International Group On Research Reactors (IGORR9)*, 2003. Sydney, Australia.
- [9] G.L. Hofman, R.G. Pahl, C.E. Lahm, D.L. Porter, Swelling behavior of U–Pu–Zr fuel, *Metall. Trans. A* 21A (1990) 517–528.
- [10] W.J. Carmack, D.L. Porter, S.L. Hayes, The EBR-II X447 high temperature U–10Zr metal alloy experiment, *Trans. Am. Nucl. Soc.* 106 (2012) 1111–1112.
- [11] T. Ogata, T. Yokoo, Development and validation of ALFUS: an irradiation behavior analysis code for metallic fast reactor fuels, *Nucl. Technol.* 128 (1999) 113–123.
- [12] Fluent Inc, FLUENT 6.2 User's Guide, Fluent Inc., Lebanon (NH), 2005.
- [13] J. Dirker, J.P. Meyer, Heat transfer coefficients in concentric annuli, *J. Heat Trans. – Trans. ASME* 124 (2002) 1200–1203.
- [14] S.J. Kim, D. Carpenter, G. Kohse, L.W. Hu, Hydride fuel irradiation in MITR-II: thermal design and validation results, *Nucl. Eng. Des.* 277 (2014) 1–14.
- [15] S. Mo, P. Hu, J. Cao, Z. Chen, H. Fan, F. Yu, Effective thermal conductivity of moist porous sintered nickel material, *Int. J. Thermophys.* 27 (2006) 304–313.
- [16] S. Simunovic, L.J. Ott, S.B. Gorti, J.A. Turner, Modeling of gap closure in uranium zirconium alloy metal fuel – a test problem (Report No. ORNL/TM-2009/248), Oak Ridge National Laboratory, Tennessee, USA, 2009.
- [17] F. Brown, J. Bull, D. Dixon, A. Forster, T. Goorley, G. Hughes, et al., MCNP – A general Monte Carlo N-Particle transport code, Los Alamos National Laboratory, Los Alamos (NM), 2003.
- [18] A.B. Gaiduchenko, Thermophysical properties of irradiated uranium–zirconium fuel, *At. Energy* 104 (2008) 5–10.
- [19] G.L. Hofman, L.C. Walters, T.H. Bauer, Metallic fast reactor fuels, *Prog. Nucl. Energy* 31 (1997) 83–110.
- [20] W. Wagner, J.R. Cooper, A. Dittmann, J. Kijima, H.-J. Kretzschmar, A. Kruse, R. Mareš, K. Oguchi, H. Sato, I. Stöcker, O. Sifner, Y. Takaishi, I. Tanishita, J. Trübenbach, Th. Wilkommen, The IAPWS industrial formulation 1997 for the thermodynamic properties of water and steam, *J. Eng. Gas Turb. Power* 122 (2000) 150–182.

[1] H. Tsai, A.B. Cohen, M.C. Billone, L.A. Niemark, Irradiation performance of U–Pu–Zr metal fuels for liquid-metal-cooled